J. Fluid Mech. (1978), *vol.* 84, *part* 4, *pp.* 743–768
Printed in Great Britain

Instability of steady natural convection in a vertical fluid layer

By R. F. BERGHOLZ
Argonne National Laboratory, Argonne, Illinois 60439

(Received 4 April 1977)

The instability of steady natural convection of a stably stratified fluid between vertical surfaces maintained at different temperatures is analysed. The linear stability theory is employed to obtain the critical Grashof and Rayleigh numbers, for widely varying levels of the stable background stratification, for Prandtl numbers ranging from 0·73 to 1000 and for the limiting case of infinite Prandtl number. The energetics of the critical disturbance modes also are investigated. The numerical results show that, if the value of the Prandtl number is in the low to moderate range, there is a transition from stationary to travelling-wave instability if the stratification exceeds a certain magnitude. However, if the Prandtl number is large, the transition, with increasing stratification, is from travelling-wave to stationary instability. The theoretical predictions are in excellent agreement with the experimental observations of Elder (1965) and of Vest & Arpaci (1969), for stationary instability, and in fair to good agreement with the experimental results of Hart (1971), for travelling-wave instability.

1. Introduction

The classical problem of natural convection in a rectangular enclosure with a fixed temperature difference between the side walls has been studied analytically, experimentally, and numerically by many investigators (Batchelor 1954; Eckert & Carlson 1961; Mordchelles-Regnier & Kaplan 1963; Elder 1965; Gill 1966; Elder 1966; Wilkes & Churchill 1966; de Vahl Davis 1968; MacGregor & Emery 1969; Oshima 1971). The properties of the flow are governed by three dimensionless parameters: the Prandtl number,

$$Pr = \nu/\kappa, \tag{1.1}$$

the aspect ratio,

$$h = H/D, \tag{1.2}$$

and either the Grashof number,

$$Gr = g\beta\Delta T D^3/\nu^2, \tag{1.3}$$

or, equivalently, the Rayleigh number,

$$Ra = PrGr, \tag{1.4}$$

where g is the gravitational acceleration, ν, κ and β are the kinematic viscosity, thermal diffusivity and coefficient of thermal expansion of the fluid, ΔT is the temperature difference between the side walls, and H and D are the height and width of the slot, respectively. In a narrow enclosure (i.e. a vertical slot with $h \gg 1$), three distinct regimes of flow can occur, each corresponding to a different range of values of the

Rayleigh number. If *Ra* is small (*conduction regime*), there is little or no variation of the fluid temperature with height, and heat is transferred between the vertical walls primarily by conduction, However, as *Ra* is increased, a stable vertical temperature gradient develops in the core of the flow (*transition regime*), and vertical velocities are progressively diminished. Finally, if *Ra* becomes sufficiently large (*boundary-layer* or *convection regime*), the flow is confined to boundary layers at the side walls, and the dominant mode of heat transfer is convection.

Instability of the base flow in the vertical slot occurs when *Gr* becomes greater than a certain critical value. The stability characteristics of the flow in the conduction regime are well established (Gershuni 1953; Birikh 1966; Rudakov 1966; Gotoh & Satoh 1966; Rudakov 1967; Vest & Arpaci 1969; Gotoh & Ikeda 1972; Birikh *et al.* 1972; Korpela, Gözüm & Baxi 1973), the most interesting being that the type of instability is determined by the magnitude of the Prandtl number. The critical disturbance modes are stationary when $Pr < 12{\cdot}7$, but they are travelling waves when $Pr \geqslant 12{\cdot}7$.

Stability analyses of the transition and boundary-layer regimes have been carried out only for specialized conditions or for restricted ranges of the governing parameters. Vest & Arpaci (1969) studied the onset of stationary instability in the boundary-layer regime and reported fair agreement between their theoretical and experimental values for the critical Grashof number. Unfortunately, the authors omitted a term, involving the vertical temperature gradient, in the linearized disturbance equations, and, hence, their results must be interpreted with caution. Birikh *et al.* (1969) and Gotoh & Mizushima (1973) found that the critical Grashof number for stationary instability increases with increasing vertical stratification, but their calculations were done for *Pr* no greater than 7·5 and only for low to moderate levels of stratification. In contrast, the computational and experimental work of Hart (1971) indicates that travelling-wave instability occurs in water ($Pr = 6{\cdot}7$) if the vertical temperature gradient is sufficiently large. Gill & Kirkham (1970) analysed the limiting case of infinite *Pr* and also found travelling waves to be the cause of instability, irrespective of the level of stratification. However, their predictions are not consistent with observations of stationary, roll-type instabilities in experiments with high Prandtl number fluids (Elder 1965; Vest & Arpaci 1969). Also, numerical solutions of the steady-state Boussinesq equations for $Pr = 1000$ have confirmed the existence of a steady, multicellular, secondary flow at values of *Gr* much less than the critical value for travelling-wave instability (de Vahl Davis & Mallinson 1975).

Clearly, while much has been learned regarding the instability of the conduction regime, our understanding of instability in the transition and boundary-layer regimes is far from complete. The seriousness of this deficiency is accentuated by the fact that the latter types of flow are most commonly encountered in practical situations.

The purpose of this study is to examine the stability properties of the transition and boundary-layer regimes in detail. Stability computations were performed over a large interval in magnitude of the stable background stratification, for Prandtl numbers ranging from 0·73 to 1000 and for the limiting case of infinite Prandtl number. In addition, the energetics of the critical disturbance modes were investigated at each computed critical point. The results show that there is a marked variation in the stability characteristics of the flow depending upon the relative magnitudes of the governing parameters. These variations are related to changes in the dominant energy sources for the instability. At low to moderate values of Pr, a transition from stationary to travelling-wave instability takes place when the vertical stratification becomes sufficiently large. However, at high Prandtl numbers, increasing the vertical stratification causes a transition from travelling-wave to stationary instability. The disturbance energy calculations indicate that instability of the flow is mechanically driven at low to moderate Prandtl numbers, if the vertical stratification is not too large, and buoyancy driven at high Prandtl numbers and at high levels of the stratification. The theoretical predictions for Gr_c are in excellent agreement with the experimental values reported by Elder (1965) and by Vest & Arpaci (1969) for stationary instabilities at both low and high Prandtl numbers, and in fair to good agreement with the experimental data of Hart (1971) for travelling-wave instability at moderate Prandtl number.

Recently, after the research reported in this paper was completed, an investigation dealing with the same problem was published by Mizushima & Gotoh (1976). Stability calculations were done for $Pr = 7{\cdot}5$ and a few values of the stratification parameter. Their results are qualitatively similar to some of those presented in this work, but, at the same time, there are significant quantitative differences. A fuller discussion of their paper is presented in §7.

2. The base flow

The geometric arrangement of the problem is illustrated schematically in figure 1. An incompressible, Newtonian fluid of kinematic viscosity ν, thermal diffusivity κ, and coefficient of thermal expansion β is contained in a vertical channel, of width D, defined in the Cartesian co-ordinate system (x, y, z) by $-\infty < x < \infty, 0 \leqslant y \leqslant D, -\infty < z < \infty$. The gravitational acceleration vector $\mathbf{g}$ acts antiparallel to the $+z$ axis. A uniform temperature gradient, $S > 0$, is maintained in the z direction along each of the channel walls, resulting in a stable vertical density stratification in the fluid at rest. The base flow is generated by applying a constant temperature difference, ΔT, between the lateral boundaries.

Using the linear equation of state

$$\rho = -\rho_0 \beta T, \tag{2.1}$$

and introducing the set of scales $[D, g\beta\Delta T D^2/\nu, \Delta T, \rho_0 g\beta\Delta T D, \nu/(g\beta\Delta T D)]$ for length, velocity, temperature, pressure, and time, respectively, the non-dimensional field equations and boundary conditions governing the fluid motion, under the Boussinesq approximation, are

$$\left.\begin{aligned} Gr(\partial\mathbf{v}/\partial t + \mathbf{v}\,.\,\nabla\mathbf{v}) &= -\nabla p + T\mathbf{k} + \nabla^2\mathbf{v},\\ \nabla\,.\,\mathbf{v} &= 0,\\ Ra(\partial T/\partial t + \mathbf{v}\,.\,\nabla T) &= \nabla^2 T,\\ \mathbf{v}(x,0,z) = 0 &= \mathbf{v}(x,1,z),\\ T(x,0,z) &= \tfrac{1}{2} + \tau z,\\ T(x,1,z) &= -\tfrac{1}{2} + \tau z. \end{aligned}\right\} \tag{2.2}$$

The velocity, $\mathbf{v} = (u, v, w)$, the pressure, p, the temperature, T, and the density, ρ, are measured relative to arbitrary reference quantities in the static state, $\mathbf{k}$ is a unit vector

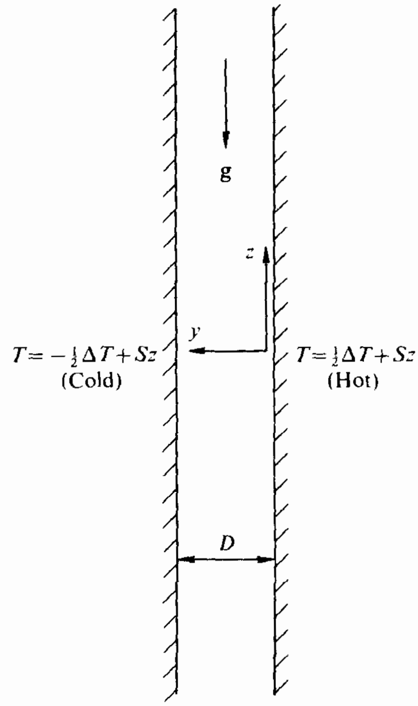

FIGURE 1. Schematic illustration of the problem geometry.

along the $+z$ axis, and t is the time. The dimensionless vertical temperature gradient τ is given by

$$\tau = SD/\Delta T. \tag{2.3}$$

Equations (2.2) yield exact solutions for the basic state of the form $\mathbf{v} = (0, 0, W(y))$, $p = p(y)$, $T = \Theta(y) + \tau z$ (see Elder 1965), where W and Θ are the real parts of

$$W(y) = (i/8\gamma^2)\,[f_1(y) - f_{-1}(y)], \tag{2.4a}$$

$$\Theta(y) = -\tfrac{1}{4}[f_1(y) + f_{-1}(y)], \tag{2.4b}$$

$$f_m(y) = \frac{\sinh\left[(1+mi)\,\gamma y\right] - \sinh\left[(1+mi)\,\gamma(1-y)\right]}{\sinh\left[(1+mi)\,\gamma\right]}, \quad m = \pm 1, \tag{2.4c}$$

$$\gamma = (\tfrac{1}{4}\tau Ra)^{\frac{1}{4}}. \tag{2.4d}$$

The cross-stream velocity and temperature profiles, $W(y)$ and $\Theta(y)$, are displayed in figure 2 for values of the stratification parameter, γ, ranging from 0·1 (conduction regime) to 10 (boundary-layer regime). Reversals in the horizontal temperature gradient occur in the central part of the channel when $\gamma \geqslant 4{\cdot}8$, and reversals in the vertical velocity are found in the same region when $\gamma > 8$. In the limit $\gamma \to 0$ $(\tau \to 0)$, $W(y)$ and $\Theta(y)$ approach the simple conduction profiles

$$W(y) = \tfrac{1}{6}[(y-\tfrac{1}{2})^3 - \tfrac{1}{4}(y-\tfrac{1}{2})], \quad \Theta(y) = -(y-\tfrac{1}{2}). \tag{2.5}$$

In the opposite limit, $\gamma \to \infty$ $(D \to \infty)$, we obtain the boundary-layer solutions, derived by Gill & Davey (1969), for the flow adjacent to a single heated wall laterally bounding a stably stratified fluid:

$$\hat{W}(\eta) = e^{-\eta}\sin\eta, \quad \hat{\Theta}(\eta) = e^{-\eta}\cos\eta, \tag{2.6}$$

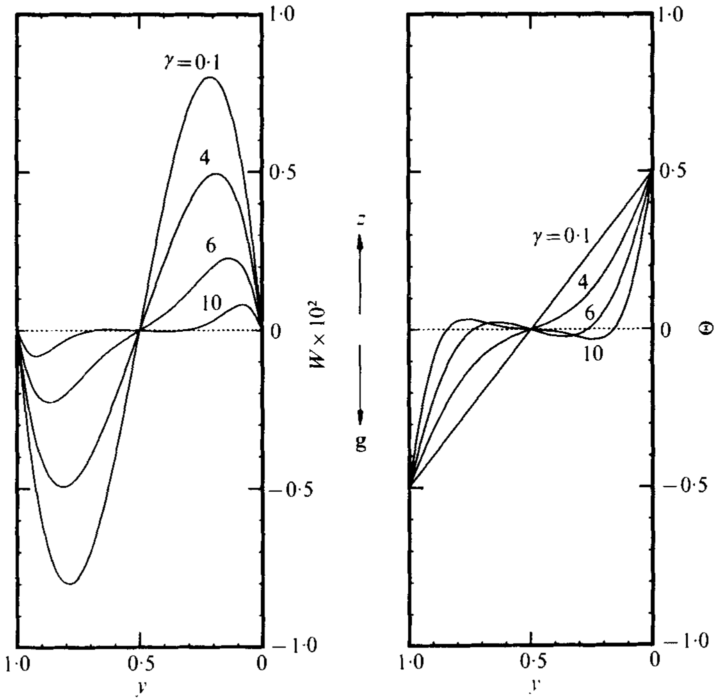

FIGURE 2. Base flow velocity ($W \times 10^2$) and temperature (Θ) profiles for various values of the stratification parameter, γ.

in which the new scaling is $\eta = \gamma y$, $\hat{W} = 4\gamma^2 W$, and $\hat{\Theta} = 2\Theta$. This boundary-layer flow is commonly referred to as the buoyancy layer.

3. Linear stability theory

Small disturbances of arbitrary form are superimposed upon the basic state in the following manner:

$$(\mathbf{v}, T, p) = (W, \Theta + \tau z, 0) + \epsilon(\mathbf{v}', \Gamma, p'), \quad \epsilon \ll 1. \tag{3.1}$$

The linearized equations governing the initial growth or decay of the disturbances are derived in the usual way by introducing (3.1) into the original Boussinesq system (2.2) and neglecting terms $O(\epsilon^2)$. Only two-dimensional disturbances in the y, z plane will be considered, even though Squire's theorem, which reduces the full three-dimensional stability problem to an equivalent two-dimensional one, is not valid unless $\tau \equiv 0$. This is not a serious restriction, because experiments have shown the basic state to be most unstable to perturbations of this type. Accordingly, all disturbance variables are functions of (y, z, t) alone, and $u' \equiv 0$. The general solution of the stability equations then can be written as a superposition of Fourier modes of the form

$$(\psi(y,z), \Gamma(y,z)) = (\phi(y), \theta(y)) \exp[i\alpha(z - ct)], \tag{3.2}$$

where the perturbation stream function ψ is defined by

$$v' = -\psi_z, \quad w' = \psi_y, \tag{3.3}$$

and the functions $\phi(y)$ and $\theta(y)$ satisfy

$$\mathscr{L}^2\phi - i\alpha Gr[(W-c)\mathscr{L}\phi - W''\phi] + \theta' = 0, \tag{3.4a}$$

$$\mathscr{L}\theta - i\alpha Ra[(W-c)\theta - \Theta'\phi] - 4\gamma^4\phi' = 0, \tag{3.4b}$$

$$\phi = \phi' = \theta = 0 \quad \text{on} \quad y = 0, 1, \tag{3.4c}$$

$$\mathscr{L} = d^2/dy^2 - \alpha^2, \tag{3.4d}$$

with primes denoting ordinary differentiation with respect to y. The wavenumber, α, is assumed to be real, and the wave speed, $c = c_r + ic_i$, is complex. Here, and in the remainder of the paper, subscripts r and i refer to the real and imaginary parts of a complex quantity, respectively. If $c_r = 0$, the disturbance mode is stationary; otherwise, it is a travelling wave. Note that in (3.4b) the stratification parameter, γ, has been substituted in place of the dimensionless vertical temperature gradient, τ, as an independent parameter of the problem. The choice is arbitrary, because γ and τ are related through (2.4d). The aspect ratio, h, could also be used, but then τ must be determined empirically as a function of Ra and h (see Hart 1971). For our purposes, this is not as convenient as specifying γ (or τ) directly.

The system (3.4a–d) defines an eigenvalue problem in which Pr, γ, Gr, and α are parameters, and

$$\lambda = -i\alpha c Gr \tag{3.5}$$

is an eigenvalue. The marginal stability boundary is simply a curve for $Gr(\alpha;\, Pr, \gamma)$ on which $\lambda_r = 0$. This curve may have one or more minima depending upon the values of Pr and γ. In addition, if the flow is subject to both stationary and travelling-wave instability, the neutral curves for each might be very different. In any event, the critical Grashof number, Gr_c, and critical wavenumber, α_c, correspond to the *absolute* minimum of $Gr(\alpha;\, Pr, \gamma)$ over all α.

It is of interest to derive the asymptotic form of the system (3.4a–d) in the limit $\gamma \to \infty$. Using the transformations $\eta = \gamma y$, $\hat{W} = 4\gamma^2 W$, $\hat{\Theta} = 2\Theta$, $\hat{\phi} = 2\gamma^3\phi$, and $\hat{\theta} = \theta$, we obtain

$$\hat{\mathscr{L}}^2\hat{\phi} - i\hat{\alpha}\hat{R}[(\hat{W}-\hat{c})\hat{\mathscr{L}}\hat{\phi} - \hat{W}''\hat{\phi}] + 2\hat{\theta}' = 0, \tag{3.6a}$$

$$\hat{\mathscr{L}}\hat{\theta} - i\hat{\alpha}\hat{R}Pr[(\hat{W}-\hat{c})\hat{\theta} - \hat{\Theta}'\hat{\phi}] - 2\hat{\phi}' = 0, \tag{3.6b}$$

$$\hat{\phi} = \hat{\phi}' = \hat{\theta} = 0 \quad \text{at} \quad y = 0, \tag{3.6c}$$

$$\hat{\phi}, \hat{\theta} \to 0 \quad \text{as} \quad y \to \infty, \tag{3.6d}$$

where

$$\hat{\mathscr{L}} = d^2/d\eta^2 - \hat{\alpha}^2,$$

and

$$\hat{R} = Gr/4\gamma^3, \quad \hat{\alpha} = \alpha/\gamma, \quad \hat{c} = 4\gamma^2 c. \tag{3.7}$$

The limit $\gamma \to \infty$ was taken with $\hat{R}$, $\hat{\alpha}$, and $\hat{c}$ fixed. Equations (3.6a–d) are precisely those given by Gill & Davey (1969) for the buoyancy layer, with $\hat{W}$ and $\hat{\Theta}$ given by (2.6). The new parameter $\hat{R}$ is the boundary layer Reynolds number.

4. Power integrals

Considerable insight into the mechanisms involved in the onset of instability can be achieved by using the global power balance to calculate the relative magnitudes of the sources and sinks of disturbance energy in the flow. Letting ϕ^* and θ^* represent the complex conjugates of ϕ and θ, the power balance is obtained by the following procedure. Multiply (3.4*a*) by ϕ^*, (3.4*b*) by θ^*, integrate over the interval $0 \leqslant y \leqslant 1$, and take the real parts of the results. This gives

$$\alpha c_i Gr E_k = Gr\Sigma_1 + \Sigma_2 + \Sigma_3, \tag{4.1a}$$

$$\alpha c_i Gr E_p = Gr(\Sigma_4 + \Sigma_5) + Pr^{-1}\Sigma_6, \tag{4.1b}$$

where

$$E_k = -\frac{1}{2}\int_0^1 \phi^*(\mathscr{L}\phi)\,dy, \tag{4.1c}$$

$$E_p = \frac{1}{2}\int_0^1 \theta^*\theta\,dy, \tag{4.1d}$$

$$\Sigma_1 = \frac{i\alpha}{4}\int_0^1 [\phi^*(\mathscr{L}_1\phi) - \phi(\mathscr{L}_1\phi^*)]\,dy, \tag{4.1e}$$

$$\Sigma_2 = -\frac{1}{4}\int_0^1 (\phi\theta^{*\prime} + \phi^*\theta')\,dy, \tag{4.1f}$$

$$\Sigma_3 = -\frac{1}{2}\int_0^1 \phi^*(\mathscr{L}^2\phi)\,dy, \tag{4.1g}$$

$$\Sigma_4 = -(4\gamma^4/Ra)\,\Sigma_2, \tag{4.1h}$$

$$\Sigma_5 = \frac{i\alpha}{4}\int_0^1 (\theta^*\phi - \theta\phi^*)\,\Theta'\,dy, \tag{4.1i}$$

$$\Sigma_6 = \frac{1}{2}\int_0^1 \theta^*(\mathscr{L}\theta)\,dy, \tag{4.1j}$$

and $\mathscr{L}_1 = W\mathscr{L} - W''$. The quantities E_k and E_p are the kinetic and potential energies of the disturbance, respectively, and $\alpha c_i Gr E_k$ and $\alpha c_i Gr E_p$ are the time rates of change of E_k and E_p. The possible energy source terms are $Gr\Sigma_1$, the rate of transfer of kinetic energy from the mean flow to the disturbance due to Reynolds stresses, Σ_2, the rate of change of kinetic energy due to buoyancy forces, $Gr\Sigma_4$, the rate of change of potential energy due to interaction of the disturbance with the vertical base flow temperature gradient, and $Gr\Sigma_5$, the rate of change of potential energy due to interaction of the disturbance with the horizontal base flow temperature gradient. Of course, for certain combinations of the governing parameters, any one of these terms can be negative, thereby representing an energy sink. The quantities Σ_3 and $Pr^{-1}\Sigma_6$ are always energy sinks: Σ_3 is the rate of loss of kinetic energy due to viscous dissipation, while $Pr^{-1}\Sigma_6$ is the rate of loss of potential energy due to heat diffusion.

5. Numerical method

High-order approximate solutions of the eigenvalue problem were obtained by Galerkin's method. The disturbance variables were expanded in the finite series

$$\phi(y) = \sum_{n=1}^{N} a_n \phi_n(y), \tag{5.1a}$$

$$\theta(y) = \sqrt{2}\sum_{n=1}^{N} b_n \sin n\pi y, \tag{5.1b}$$

where the ϕ_n are members of a complete set of eigenfunctions (sometimes called beam functions) satisfying the fourth-order equation $\phi_n^{(\mathrm{iv})} = \mu_n^4\phi_n$, with $\phi_n = \phi_n' = 0$ on

$y = 0, 1$. The eigenvalues μ_n are roots of the transcendental equation $\cosh \mu_n \cos \mu_n = 1$. The procedure for determining the unknown coefficients a_n and b_n is straightforward. Let $\mathscr{L}_1[\Sigma a_n \phi_n, \Sigma b_n \theta_n] = 0$ and $\mathscr{L}_2[\Sigma a_n \phi_n, \Sigma b_n \theta_n] = 0$ be symbolic representations of the equations resulting from substitution of the approximate solutions (5.1 *a, b*) into the ordinary differential equations (3.4 *a, b*). Now form the successive inner products

$$\left.\begin{aligned} \langle \phi_m, \mathscr{L}_1[\Sigma a_n \phi_n, \Sigma b_n \theta_n]\rangle &= 0, \quad m = 1, 2, \ldots, N, \\ \langle \theta_m, \mathscr{L}_2[\Sigma a_n \phi_n, \Sigma b_n \theta_n]\rangle &= 0, \quad m = 1, 2, \ldots, N, \end{aligned}\right\} \tag{5.2}$$

where

$$\langle f, g\rangle = \int_0^1 f(y)\, g(y)\, dy. \tag{5.3}$$

This reduces the ordinary differential system to the complex generalized algebraic eigenvalue problem

$$\mathbf{A}\mathbf{x} = \lambda \mathbf{B}\mathbf{x}, \tag{5.4}$$

where $\mathbf{x}^{\mathrm{T}} = (\mathbf{a}, \mathbf{b}) = (a_1, a_2, \ldots, a_N, b_1, b_2, \ldots, b_N)$ is the transpose of the column vector $\mathbf{x}$. The coefficient matrices $\mathbf{A}$ and $\mathbf{B}$ are defined in the appendix. Both are of dimension $2N \times 2N$, $\mathbf{A}$ is complex, and $\mathbf{B}$ is real and symmetric. The elements of these matrices were computed from simple algebraic expressions obtained by exact evaluation of the inner product integrals. Details of the integration method are given in von Kerczek (1973) and in Bergholz (1976).

A complex analogue of the QZ algorithm developed by Moler & Stewart (1973) was used to solve the eigenvalue problem (5.4). For given values of *Pr* and γ, neutral stability curves for both stationary and travelling-wave disturbances were found. Points on these curves were obtained by applying a secant method iteration either to *Gr*, with α fixed, or to α, with *Gr* fixed, until the condition $\hat{\lambda}_r = 0$ was satisfied to within a specified error. The eigenvalue $\hat{\lambda}$ was the eigenvalue with the largest real part for the particular type of disturbance in question. The errors in α and *Gr* at the neutral point are estimated to be less than 1 %. The critical values of α and *Gr* were determined by polynomial interpolation of points near the minimum of the neutral curve. The critical Grashof number for the flow is $Gr_c = \min(Gr_c^S, Gr_c^T)$, where Gr_c^S and Gr_c^T are the critical Grashof numbers for the stationary and the travelling-wave disturbances, respectively.

The convergence of the Galerkin method was tested by examining the variation of $\hat{\lambda}$ with N, the number of terms retained in the expansions (5.1 *a, b*). Selected results are displayed in table 1 for several combinations of the governing parameters. The fastest convergence was achieved when the disturbance was stationary or when the product αGr was relatively small. Satisfactory accuracy throughout the entire parameter range was attained with N ranging from 24 to 30.

The power integral components E_k, E_p and $\Sigma_1, \ldots, \Sigma_6$ are defined in the appendix in terms of the coefficient matrices, $\mathbf{A}$ and $\mathbf{B}$, and the eigenvectors, $\mathbf{a}$ and $\mathbf{b}$. The magnitudes of these components were computed at every critical point, and (4.1 *a, b*) yielded an identity to at least six significant figures in most cases.

$Pr = 5;\ \gamma = 1;\ \alpha = 2{\cdot}77;\ Gr = 8 \times 10^3$

N	λ_r	$c \times 10^3$
10	0·34113	0
14	0·53056	0
18	0·52993	0
22	0·52977	0
26	0·52973	0
30	0·52972	0

$Pr = 0{\cdot}73;\ \gamma = 6;\ \alpha = 2{\cdot}78;\ Gr = 1{\cdot}86 \times 10^5$

N	λ_r	$c \times 10^3$
10	−0·75870	1·20454
14	0·67526	1·20577
18	0·72347	1·20594
22	0·71056	1·20590
26	0·70154	1·20589
30	0·69758	1·20588

$Pr = 6{\cdot}7;\ \gamma = 4{\cdot}2;\ \alpha = 1{\cdot}07;\ Gr = 1{\cdot}9 \times 10^4$

N	λ_r	$c \times 10^3$
10	0·06319	4·33032
14	0·03395	4·33148
18	0·03189	4·33161
22	0·03158	4·33162
26	0·03151	4·33163
30	0·03149	4·33163

$Pr = 1000;\ \gamma = 9;\ \alpha = 4{\cdot}37;\ Gr = 3{\cdot}5 \times 10^2$

N	λ_r	$c \times 10^3$
10	0·01111	0
14	0·01098	0
18	0·01097	0
22	0·01097	0
26	0·01097	0
30	0·01097	0

TABLE 1. Selected results of convergence tests of the Galerkin method.

6. Results

The effects of the vertical stratification upon the critical Grashof number, Rayleigh number, wavenumber, and wave speed were investigated for ten finite values of the Prandtl number ranging from 0·73 to 1000 as well as for the limiting condition of infinite Pr. Also, the relative strengths of the energy source terms ($Gr\Sigma_1$, Σ_2, $Gr\Sigma_4$, and $Gr\Sigma_5$) for the critical disturbance modes were evaluated as functions of γ and Pr. Finally, a series of computations was performed to obtain the critical parameters for those specific values of Pr and h found in the experimental work of Elder (1965), Vest & Arpaci (1969), and Hart (1971).

In the following two subsections, we first present the results for the Prandtl numbers of low to moderate magnitude, and then those for the larger Prandtl numbers.

6.1. *Low to moderate Prandtl numbers* ($Pr = 0{\cdot}73$–$12{\cdot}7$)

The variation of Gr_c with γ and Pr is illustrated in figure 3. The dashed and solid curves represent $Gr_c^S(\gamma; Pr)$ and $Gr_c^T(\gamma; Pr)$ for the stationary and the travelling modes, respectively, and the curve markers indicate the computed points. The critical curves in these and subsequent figures were obtained by cubic spline interpolation of the associated critical points.

To begin, consider the behaviour of Gr_c^S, as γ increases, for the Prandtl numbers 0·73–12·7. In this Prandtl number range, there is only a weak dependence of Gr_c^S upon Pr, and so, for the sake of clarity, only a single dashed curve (for $Pr = 5$) was drawn. The greatest deviation from this curve occurs for $Pr = 0{\cdot}73$, but the difference is less than 3 %. The calculated values of Gr_c^S are in close agreement with those reported previously for the stationary case (Korpela *et al.* 1973, for $\gamma = 0$; Birikh *et al.* 1969, and Gotoh & Mizushima 1973, for $0 < \gamma \leqslant 4$). However, in spite of the agreement with Gotoh & Mizushima (1973) for $\gamma = 1, 2, 3$ and 4, their asymptotic formula for 'large' γ,

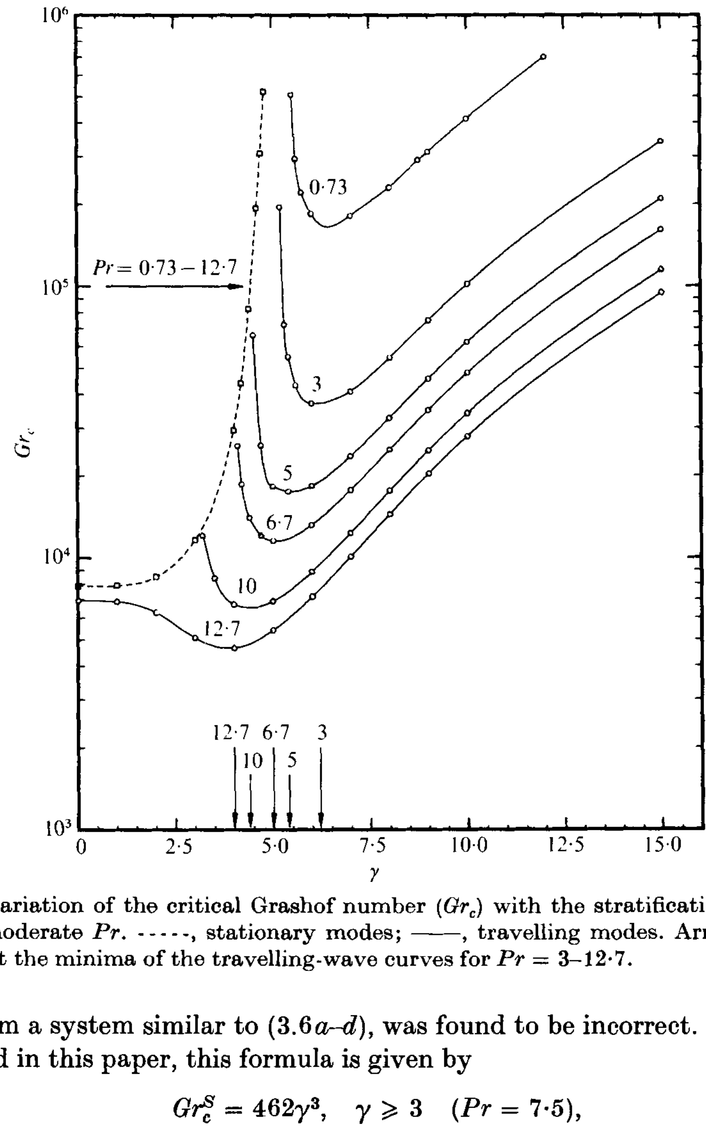

FIGURE 3. Variation of the critical Grashof number (Gr_c) with the stratification parameter (γ) for low to moderate Pr. - - - - -, stationary modes; ——, travelling modes. Arrows indicate the values of γ at the minima of the travelling-wave curves for Pr = 3–12·7.

derived from a system similar to (3.6*a*–*d*), was found to be incorrect. In terms of the scaling used in this paper, this formula is given by

$$Gr_c^S = 462\gamma^3, \quad \gamma \geqslant 3 \quad (Pr = 7{\cdot}5), \tag{6.1}$$

the coefficient being determined from the computed values of Gr_c^S at $\gamma = 3$ and 4. A direct computation was made for $Pr = 7{\cdot}5$, $\gamma = 4{\cdot}8$, which gave $Gr_c^S = 5{\cdot}21 \times 10^5$, whereas (6.1) predicts $Gr_c^S = 5{\cdot}11 \times 10^4$. The large discrepancy between the two values for Gr_c^S might be due to the fact that (6.1) was obtained using values of γ which are rather small. Yet, it is also possible that (3.6*a*–*d*), together with the asymmetric boundary-layer profiles, $\hat{W}$ and $\hat{\Theta}$, simply do not admit stationary solutions. None were found by Gill & Davey (1969) in their study of the buoyancy layer. If such solutions to (3.6*a*–*d*) do not exist, then the asymptotic relations (3.7), from which (6.1) follows, are meaningless in the stationary case.

Returning to the discussion of figure 3, it can be seen that the flow is rapidly stabilized against stationary disturbances as the vertical stratification increases, and that, if $Pr < 12{\cdot}7$, $Gr_c = Gr_c^S$ if the stratification is sufficiently small. However, if γ exceeds

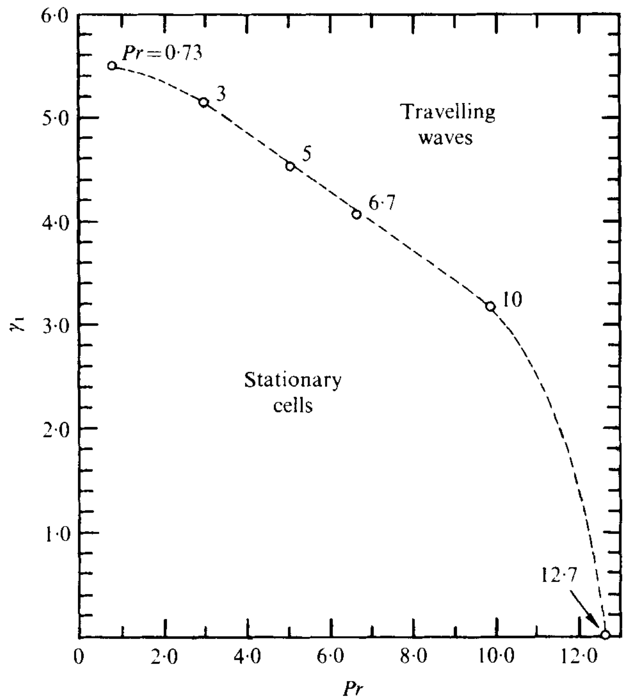

FIGURE 4. The magnitude (γ_1) of the stratification parameter, at the point of transition from stationary to travelling-wave instability, as a function of the Prandtl number (Pr).

a certain value, γ_1, which depends upon Pr, travelling-wave disturbances govern the onset of instability, and $Gr_c(= Gr_c^T)$ is given by the solid curve for the appropriate value of Pr. To avoid confusion, the segments of the curves for Gr_c^T which extend above the points of intersection with the dashed curve for Gr_c^S are not shown. The transition points for $Pr = 0·73$ and 3 occur at very large values of Gr_c, and so they must be estimated by extrapolation of the curves for Gr_c^S and Gr_c^T. Detailed calculations were not pursued when Gr_c became greater than about $9·3 \times 10^5$. The critical Grashof number for $Pr = 12·7$ is determined entirely by travelling-wave disturbances, which is consistent with the fact that 12·7 is the limiting value of Pr for onset of travelling-wave instability in the conduction regime (Korpela *et al.* 1973).

The curve for $\gamma_1(Pr)$, plotted in figure 4, defines the boundary between the stationary and travelling-wave domains in the low to moderate Prandtl number case. The magnitude of γ_1 decreases as Pr increases, the variation being almost linear from $Pr = 3$ to $Pr = 10$. Points below the curve represent parameter combinations (γ, Pr) for which $Gr_c = Gr_c^S$, while points above the curve are those for which $Gr_c = Gr_c^T$.

After transition to travelling-wave instability, Gr_c declines sharply at first, then passes through a minimum at a particular value of γ, designated by γ_2, and finally increases continuously with increasing γ. The minimum points, $\gamma_2(Pr)$, of the travelling-wave curves are indicated by the arrows in figure 3.

The process of transition from stationary to travelling-wave instability is illustrated in figure 5 for $Pr = 10$. In this figure, the neutral curves for the stationary and travelling modes are shown for values of γ near the transition value γ_1. At $\gamma = 3·1$, the minimum

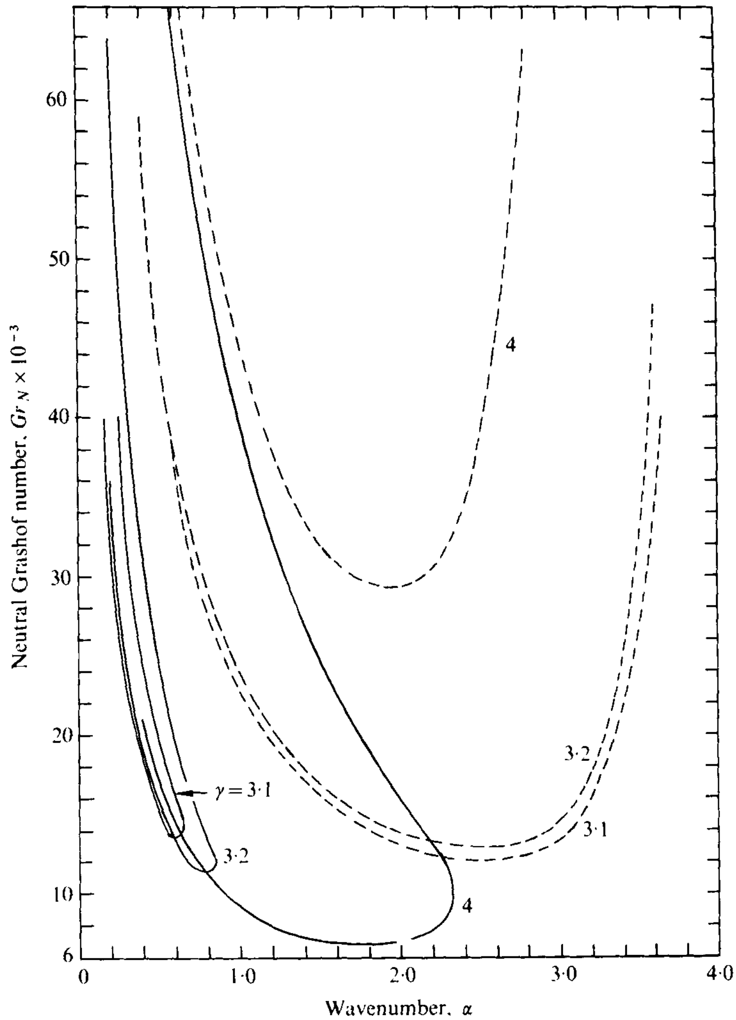

FIGURE 5. Neutral stability curves for values of γ near the point of transition from stationary to travelling-wave instability for $Pr = 10$. -----, stationary modes; ——, travelling modes.

point of the stationary (dashed) curve is lower than that of the travelling-wave (solid) curve and, therefore, $Gr_c = Gr_c^S$. However, if γ is increased slightly to 3·2, the minimum point of the travelling-wave curve extends downward to a level below the minimum of the stationary curve. Thus, at $\gamma = 3{\cdot}2$, $Gr_c = Gr_c^T$. The two curves continue their displacement relative to one another as γ is further increased to a value of 4. Near $\gamma = 5$ (not shown in figure 5), the minimum point of the travelling-wave curve ceases its downward extension and begins to move upward with increasing γ.

Another interesting type of transition can be found in the travelling-wave neutral curve for $Pr = 0{\cdot}73$ when γ is near 8·75. As shown in figure 6, the neutral curve has two minima, one at $\alpha = 2{\cdot}7$, the other at $\alpha = 4{\cdot}6$. As γ is increased or decreased from the value 8·75, the two minima shift their position relative to one another in such a way that, when $\gamma < 8{\cdot}75$, the high-wavenumber minimum determines the values of Gr_c and α_c, whereas the low-wavenumber minimum determines these values when $\gamma \geqslant 8{\cdot}75$.

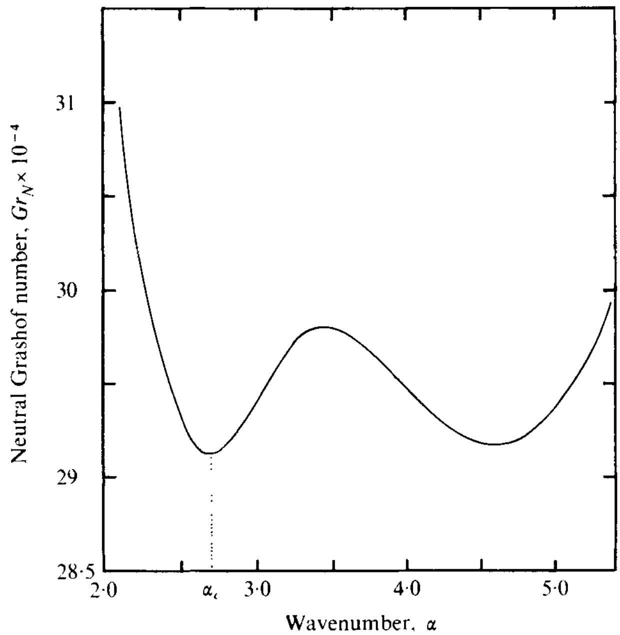

FIGURE 6. Neutral stability curve showing the low- and high-wavenumber minima for the travelling modes for $Pr = 0{\cdot}73$ at $\gamma = 8{\cdot}75$. The absolute minimum is the low-wavenumber minimum at $\alpha_c = 2{\cdot}7$.

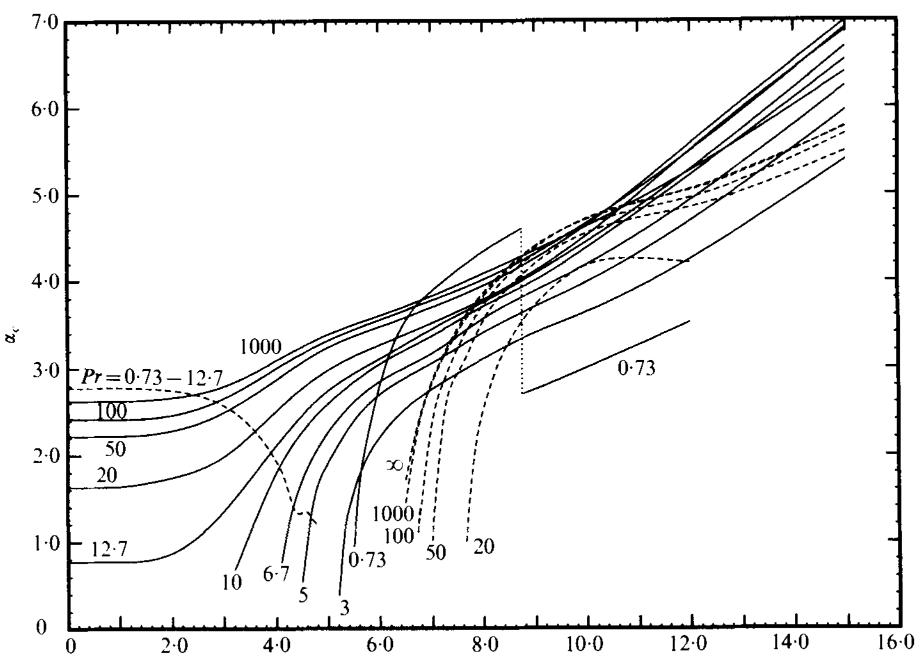

FIGURE 7. Variation of the critical wavenumber (α_c) with the stratification parameter (γ) for all values of Pr. - - - - -, stationary modes; ——, travelling modes.

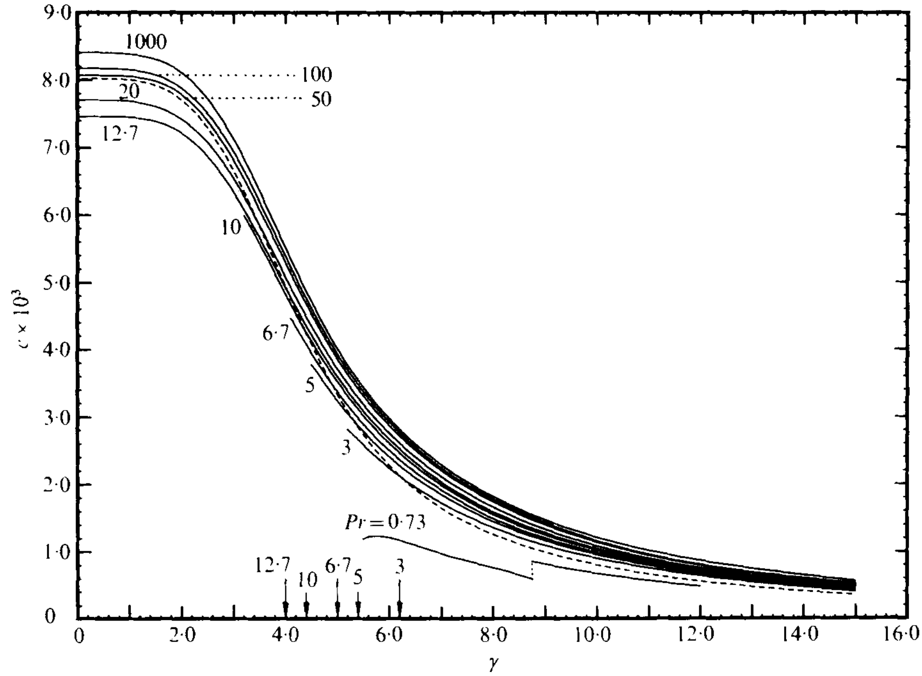

FIGURE 8. Variation of the critical wave speed ($c \times 10^3$) with the stratification parameter (γ) for all values of Pr. - - - - -, maximum base flow velocity, $\overline{W}$; ——, critical wave speeds. Arrows denote the values of γ at which $c = \overline{W}$ for $Pr = 3$ to $12{\cdot}7$.

Both Nachtsheim (1963), in his study of the natural convection boundary layer on a vertical plate, and Gill & Davey (1969), in their investigation of the buoyancy layer, found double minima in the neutral stability curves at low Pr. They showed that the low-wavenumber minimum disappears when the thermal disturbances, and, consequently, the effects of buoyancy, are neglected. Thus, the high-wavenumber minimum is associated with the purely hydrodynamic stability problem for the base flow velocity profile alone. In the case of the buoyancy layer ($\gamma \rightarrow \infty$), the low-wavenumber minimum gives the critical values of $\hat{\alpha}$ and $\hat{R}$ for all $Pr \geqslant 0{\cdot}72$. In contrast, the results of the present work for $Pr = 0{\cdot}73$ show that the high-wavenumber minimum still dominates if $\gamma < 8{\cdot}75$. Presumably, there are upper limiting values of γ for the high-wavenumber minimum for slightly greater values of Pr. However, this limiting value must decrease rapidly with increasing Pr, because our results also show that the low-wavenumber minimum establishes the critical point, for all values of γ in the travelling-wave domain, if $Pr \geqslant 3$.

The dependence of the critical wavenumber, α_c, on γ and Pr is displayed in figure 7. Just as for Gr_c^S, a single dashed curve (for $Pr = 5$) was drawn for α_c^S for $0{\cdot}73 \leqslant Pr \leqslant 12{\cdot}7$, and α_c is governed by this curve up to the starting point of the travelling-wave (solid) curve for the given value of Pr. We see that, in general, α_c^S decreases as γ increases for $\gamma \leqslant \gamma_1(Pr)$, except for a very small increase near $\alpha_c = 1{\cdot}34$. The stationary curve was not extended beyond a value of α_c^S of about $1{\cdot}1$, because Gr_c^S had become very large at this point. For $\gamma > \gamma_1$, $\alpha_c = \alpha_c^T$, which increases rapidly with increasing γ in the interval $\gamma_1 < \gamma \leqslant \gamma_2$ and then more gradually for $\gamma > \gamma_2$. The

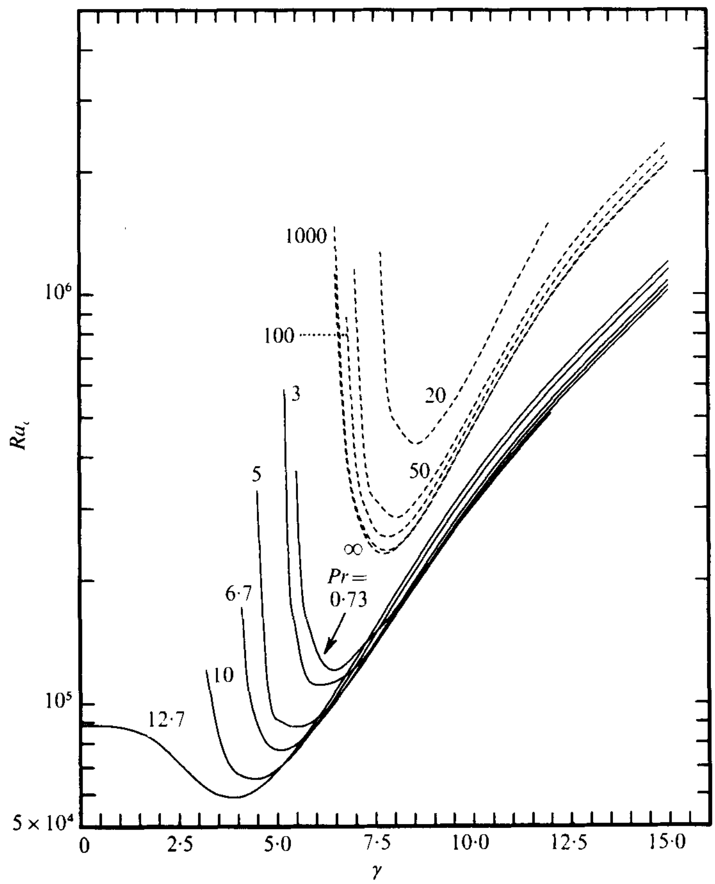

FIGURE 9. Variation of the critical Rayleigh number (Ra_c) with the stratification parameter (γ) for selected values of Pr. -----, stationary modes for large Pr; —— -, travelling modes for low to moderate Pr.

sharp drop in α_c^T at $\gamma = 8{\cdot}75$ for $Pr = 0{\cdot}73$ is due to the emergence of the low-wave-number minimum at $\alpha_c^T = 2{\cdot}7$ (see figure 6).

Additional information regarding the nature of the travelling-wave instability can be obtained from figure 8, which shows the variation of the critical wave speed, c, with γ for the various values of Pr. The dashed curve in this figure gives the maximum velocity ($\overline{W}$) of the base flow as a function of γ. The curves for the travelling waves, for $0{\cdot}73 \leqslant Pr \leqslant 12{\cdot}7$, originate at the transition points given by $\gamma_1(Pr)$ and at each of these points $c < \overline{W}$. As γ increases, c decreases in a manner similar to that of $\overline{W}$. The curves for $Pr = 3$ to $12{\cdot}7$ eventually intersect the curve for $\overline{W}$, with c being greater than $\overline{W}$ thereafter. The points at which $c = \overline{W}$ are marked by the arrows in figure 8. Referring back to figure 3, we find that these points correspond almost exactly to the minima of the curves for Gr_c^T in the travelling-wave domain. It is well known that the critical wave velocity must be less than the maximum velocity of the base flow in the case of inviscid, homogeneous, parallel shear flows. Therefore, the condition $c > \overline{W}$ must be due to the action of buoyancy forces arising from the base flow temperature field. Finally, we see that the curve for $Pr = 0{\cdot}73$, which begins at a value of c

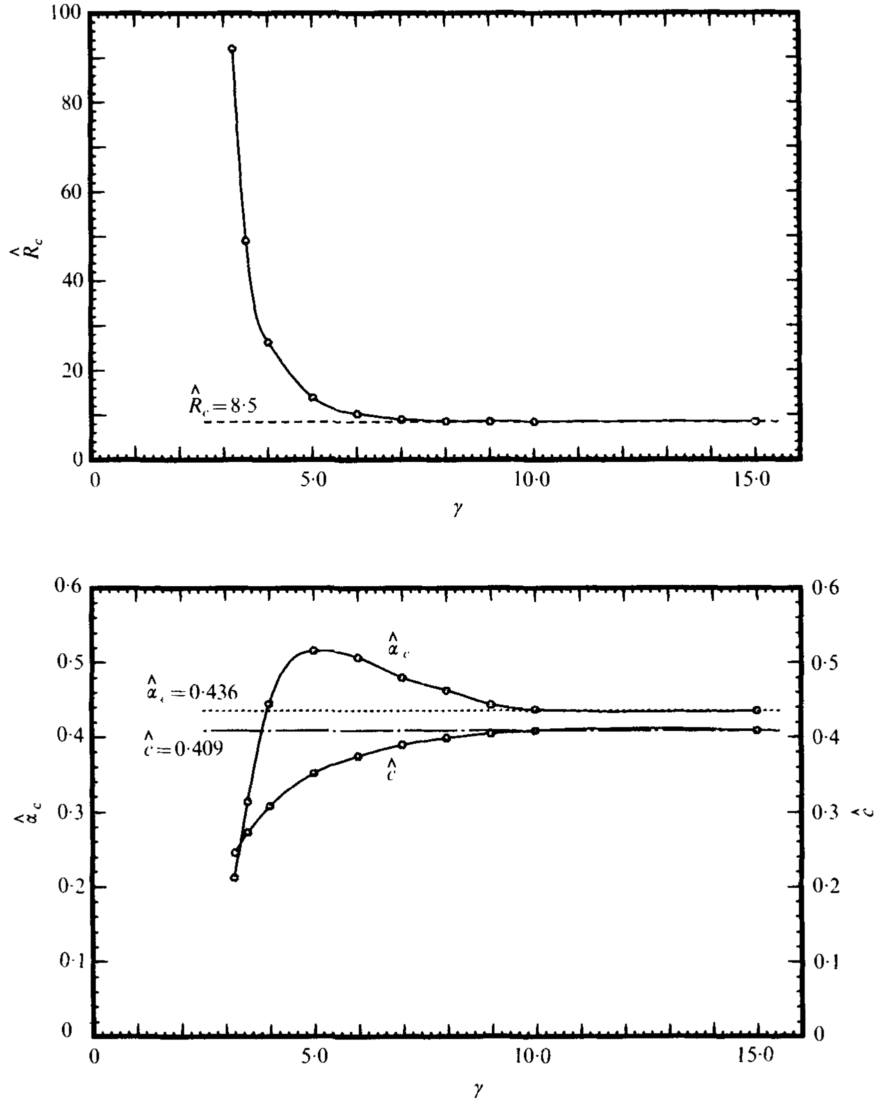

FIGURE 10. Convergence of the critical Reynolds number ($\hat{R}_c$), wavenumber ($\hat{\alpha}_c$), and wave speed ($\hat{c}$) (for finite γ) to their respective asymptotic values for the buoyancy layer ($\gamma \to \infty$). The curves for $\hat{R}$, $\hat{\alpha}$ and $\hat{c}$, computed from (3.7), and the asymptotes, obtained from Gill & Davey (1969), are for $Pr = 10$.

	High wavenumber: $\gamma = 8$	Low wavenumber: $\gamma = 10$
$\hat{R}$	112·6 (109)	103·8 (101)
$\hat{\alpha}$	0·541 (0·502)	0·300 (0·281)
$\hat{c}$	0·195 (0·200)	0·271 (0·281)

TABLE 2. Critical parameters for the high- and low-wavenumber minima for $Pr = 0{\cdot}73$. The parenthetical values are from Gill & Davey (1969) for $Pr = 0{\cdot}72$.

γ	α_c	$Gr_c \times 10^{-3}$	$c \times 10^3$	$Gr\Sigma_1$	Σ_2	$Gr\Sigma_4$	$Gr\Sigma_5$
				$Pr = 0{\cdot}73$			
1·0	2·80	8·07	0	0·9399	0·0601	−0·0002	1·0002
3·0	2·78	11·47	0	1·0084	−0·0084	0·0022	0·9978
4·4	1·21	81·86	0	1·2202	−0·2202	0·3666	0·6334
5·5	0·95	507·72	1·192	1·1450	−0·1450	0·1077	0·8923
6·0	2·78	184·62	1·206	1·0615	−0·0615	0·0277	0·9723
8·0	4·33	230·63	0·763	0·8574	0·1426	−0·0552	1·0552
8·75	2·70	291·21	0·855	0·4534	0·5466	−0·2075	1·2075
12·0	3·52	700·90	0·482	0·3947	0·6053	−0·2365	1·2365
				$Pr = 5{\cdot}0$			
1·0	2·77	7·90	0	0·8153	0·1847	−0·0001	1·0001
3·0	2·57	11·59	0	0·9220	0·0078	−0·0039	1·0039
4·4	1·33	82·59	0	1·2439	−0·2439	0·1894	0·8103
4·6	1·34	193·99	0	1·2039	−0·2039	0·2916	0·7083
4·7	1·26	307·58	0	1·1826	−0·1826	0·3229	0·6771
4·8	1·20	520·46	0	1·1561	−0·1561	0·2696	0·7304
4·5	0·54	66·14	3·779	−0·0770	1·0770	−0·0522	1·0522
4·7	1·38	25·81	3·550	−0·1315	1·1316	−0·0655	1·0656
5·0	1·90	19·29	3·235	−0·1579	1·1579	−0·0898	1·0898
5·4	2·30	17·54	2·863	−0·1551	1·1551	−0·1268	1·1271
6·0	2·69	18·36	2·402	−0·1322	1·1324	−0·1877	1·1883
8·0	3·40	32·71	1·450	−0·1019	1·1019	−0·3468	1·3470
10·0	3·98	62·35	0·957	−0·1103	1·1104	−0·3908	1·3908
15·0	5·96	209·72	0·426	−0·1117	1·1117	−0·3925	1·3925
				$Pr = 12{\cdot}7$			
1·0	0·77	6·89	7·448	0·0193	0·9807	−0·0005	1·0005
3·0	1·35	5·06	6·342	−0·0174	1·0174	−0·0310	1·0313
4·0	2·10	4·66	4·926	−0·0756	1·0756	−0·0735	1·0738
5·0	2·73	5·41	3·594	−0·0887	1·0888	−0·1469	1·1470
7·0	3·44	10·09	2·033	−0·0578	1·0578	−0·3660	1·3660
9·0	4·08	20·40	1·278	−0·0582	1·0582	−0·4541	1·4542
15·0	6·69	94·43	0·463	−0·0610	1·0610	−0·4593	1·4594
				$Pr = 1000$			
1·0	2·62	0·251	8·385	−0·0011	1·0011	−0·0003	1·0002
4·0	3·08	0·311	5·524	−0·0015	1·0015	−0·0621	1·0613
6·0	3·60	0·547	2·973	−0·0010	1·0010	−0·2412	1·2408
8·0	4·08	1·059	1·820	−0·0009	1·0009	−0·4453	1·4425
12·0	5·26	3·340	0·866	−0·0011	1·0011	−0·5706	1·5710
7·0	2·81	0·310	0	−0·0030	1·0030	−0·3615	1·3599
8·0	3·81	0·240	0	−0·0016	1·0016	−0·8352	1·8378
9·0	4·37	0·319	0	−0·0015	1·0015	−1·0171	2·0182
12·0	5·04	0·989	0	−0·0023	1·0023	−0·6832	1·6832

TABLE 3. Selected values of the critical parameters and power integral components.

considerably less than $\overline{W}$, does not intersect the $\overline{W}$ curve within the range of γ considered. This is to be expected, because the thermal disturbances tend to be heavily damped at low values of Pr. (Note the small jump at c in $\gamma = 8{\cdot}75$, the point at which the low-wavenumber minimum determines Gr_c and α_c.)

It is also informative to examine the behaviour of $Ra_c^T(\gamma;\, Pr)$ in the travelling-wave regime for $0{\cdot}73 \leqslant Pr \leqslant 12{\cdot}7$ (see the solid curves in figure 9). In the interval $\gamma_1 \leqslant \gamma \leqslant \gamma_2$, there is a significant dependence of Ra_c^T, as well as Gr_c^T, upon Pr. However, in the domain $\gamma > \gamma_2$, the curves for Ra_c^T are almost coincident, although Ra_c^T increases slightly with Pr at any given value of γ. Such a weak influence of Pr on Ra_c^T is another indication that buoyancy forces are the dominant source of instability when the vertical stratification becomes sufficiently large.

To verify the asymptotic relations (3.7), comparisons were made with the results obtained by Gill & Davey (1969) for the buoyancy layer. For the case $Pr = 10$ ($\gamma \rightarrow \infty$), Gill & Davey found $\hat{R}_c = 8{\cdot}50$, $\hat{\alpha}_c = 0{\cdot}436$, $\hat{c} = 0{\cdot}409$. Using (3.7) and our computed values for Gr_c^T, α_c^T, and c for $Pr = 10$, the values of $\hat{R}_c$, $\hat{\alpha}_c$, and $\hat{c}$ for finite γ were calculated. The results are displayed in figure 10. At $\gamma = 8$, the critical Reynolds number, $\hat{R}_c$, is within about 1 % of its asymptotic value and, for $\gamma > 10$, the values of all of the critical parameters are identical with those for the buoyancy layer. In table 2, $\hat{R}_c$, $\hat{\alpha}_c$, and $\hat{c}$ for $Pr = 0{\cdot}73$ are listed for both the high- and the low-wavenumber critical points. The corresponding values for the buoyancy layer, for $Pr = 0{\cdot}72$, are given in parentheses. Again, the agreement at large γ is rather good. Thus we can conclude that the asymptotic results for the buoyancy layer are valid for the vertical slot in the travelling-wave regime, at least for low to moderate Prandtl number, if γ is sufficiently large.

The power integral computations provided a significant amount of information about the energetics of the critical disturbance modes in the various domains of instability. A sampling of critical parameter values and relative magnitudes of the power integral source terms are recorded in table 3. Equations (4.1 a, b) were normalized by setting the viscous and thermal dissipation terms, Σ_3 and $Pr^{-1}\Sigma_6$, equal to -1. Therefore, the sums $Gr\Sigma_1 + \Sigma_2 - 1$ and $Gr\Sigma_4 + Gr\Sigma_5 - 1$ should be zero, or very near zero, at the critical points. At present, attention is restricted to the results for $Pr = 0{\cdot}73$, 5, and 12·7. As expected, we find that the stationary disturbances ($c_r = 0$) derive most of their energy from the mean flow through the Reynolds stress production term, $Gr\Sigma_1$. Thus, the stationary modes for low to moderate Pr are essentially instabilities resulting from the viscous shear at the midplane of the slot. However, note that when γ is small (conduction regime) there is also a positive contribution to the disturbance kinetic energy from the work of buoyancy forces, as indicated by the positive values for Σ_2 at $\gamma = 1$. Similar results for the conduction regime for $Pr = 0{\cdot}73$ and 6·7 were obtained by Hart (1971). As γ increases, Σ_2 decreases and eventually becomes negative, but an interesting reversal in this trend can be seen in the interval $4{\cdot}6 \leqslant \gamma \leqslant 4{\cdot}8$ for $Pr = 5$. As mentioned above, in this interval, α_c increases slightly and then declines at a slower rate than before (see figure 7). It is possible that Σ_2 again will become positive at larger values of γ, but more extensive computations would be needed to verify this.

In the travelling-wave regime, the Prandtl number plays a much more influential role in determining the mechanics of the instability. In the low Prandtl number case ($Pr = 0{\cdot}73$), $Gr\Sigma_1$ is the dominant source term when $\gamma < 8{\cdot}75$. Even in the domain $\gamma \geqslant 8{\cdot}75$, where the buoyancy term Σ_2 predominates, the Reynolds stress is still an important contributor to the disturbance kinetic energy. In contrast, instability at the higher Prandtl numbers, $Pr = 5$ and 12·7, is entirely buoyancy driven, because $Gr\Sigma_1$ is always negative, at least for the values of γ investigated, and Σ_2 is always greater than 1. Also, note that $|Gr\Sigma_1|$ and Σ_2 are greatest at values of γ near the minimum points of the curves for Gr_c^T (see figure 3).

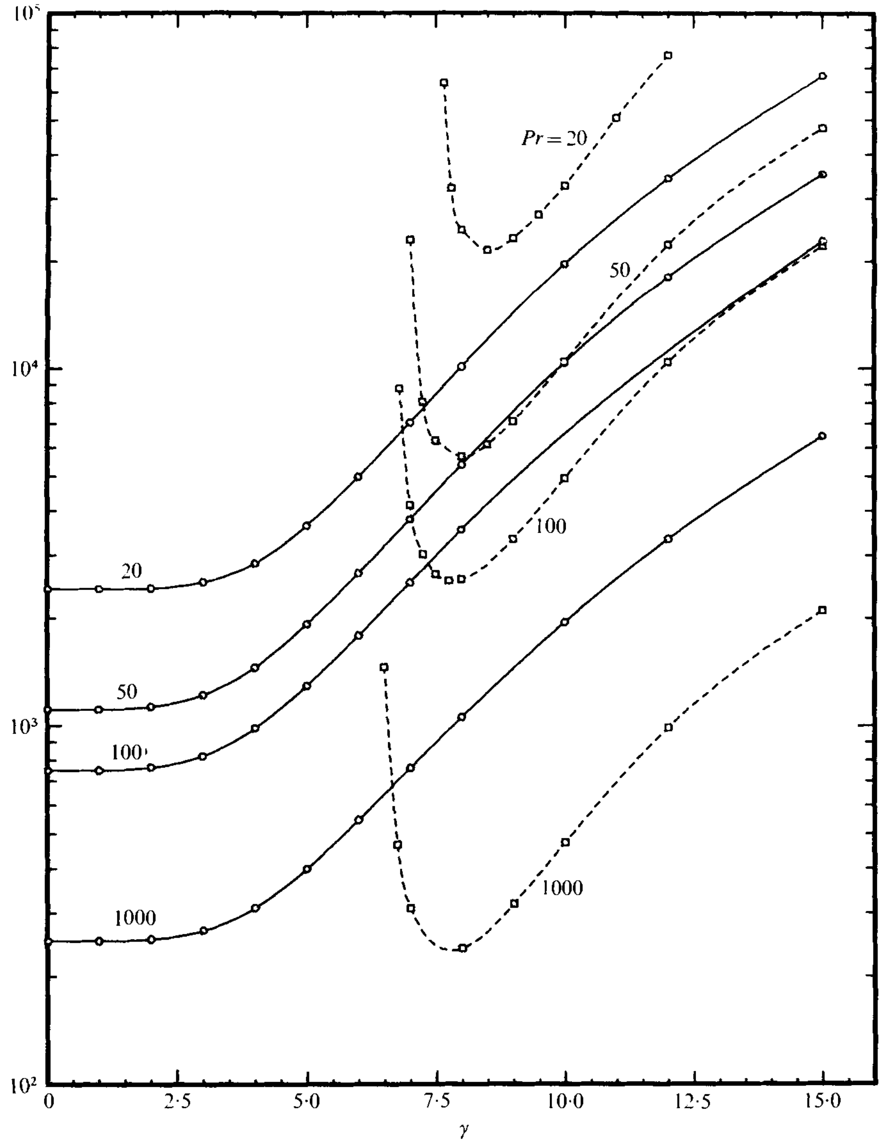

FIGURE 11. Variation of the critical Grashof number (Gr_c) with the stratification parameter (γ) for large Pr. - - - - -, stationary modes; ——, travelling modes.

6.2. *Large Prandtl numbers* ($Pr = 20$–1000)

If the Prandtl number is large, increasing the vertical stratification induces a transition in the mode of instability opposite to that found at low to moderate Prandtl numbers. This behaviour is illustrated in figure 11, which shows the Gr_c curves for $Pr = 20$–1000. It can be seen that, when $Pr \geqslant 50$, $Gr_c = Gr_c^T$ if $\gamma < \gamma_1$, but $Gr_c = Gr_c^S$ if $\gamma > \gamma_1$, where, as before, $\gamma_1(Pr)$ denotes the transition value of γ. The values of γ_1 are estimated to be $\gamma_1(50) \simeq 8{\cdot}2$, $\gamma_1(100) \simeq 7{\cdot}3$, and $\gamma_1(1000) \simeq 6{\cdot}6$. The travelling-wave curve for $Pr = 1000$ is very close to that obtained by Gill & Kirkham (1970), who analysed the stability problem in the particular limit $Pr \to \infty$ with $Pr^{\frac{1}{2}}Gr$ fixed. However, the stationary curves for $Pr = 20$–1000 have not previously been found. These curves have the same shape as those for Gr_c^T at low to moderate Pr, and, as Pr increases, their minima tend to occur at a nearly constant value of $\gamma_2 \simeq 7{\cdot}75$.

The large Pr travelling-wave results for α_c^T and c (see figures 7 and 8) are qualitatively similar to those for $Pr = 12{\cdot}7$, except that, owing to the enhanced effects of buoyancy, the critical wave velocities for $Pr = 50$–1000 are always greater than the maximum velocity of the base flow. Also, note that the α_c^T curve for $Pr = 1000$ has a smaller slope at large γ than the corresponding curves for the lower Prandtl numbers. This result is consistent with the variation of $\hat{\alpha}_c$ with Pr in the buoyancy layer. Gill & Davey (1969) found $\hat{\alpha}_c = 0{\cdot}463$ for $Pr = 100$ and $\hat{\alpha}_c = 0{\cdot}417$ for $Pr = \infty$, whereas, using our calculated values for α_c^T at $\gamma = 15$, and the asymptotic formula $\hat{\alpha}_c = \alpha_c^T/\gamma$, we obtain $\hat{\alpha}_c = 0{\cdot}461$ at $Pr = 100$ and $\hat{\alpha}_c = 0{\cdot}427$ at $Pr = 1000$.

Near the transition points, the trend of the large Pr curves for α_c^S is the same as that of the α_c^T curves for the Prandtl numbers $0{\cdot}73$ to 10, but, when the vertical stratification becomes sufficiently large, α_c^S increases, with increasing γ, at a slower rate than does α_c^T.

The critical Rayleigh number, $Ra_c^S(\gamma; Pr)$, for the large Prandtl number stationary modes behaves in the manner shown by the dashed curves in figure 9. For all values of γ, the dependence of Ra_c upon Pr becomes progressively weaker as Pr increases. This result suggests that the proper limit for the stationary modes is $Pr \to \infty$ with Ra fixed ($Gr \to 0$). In this limit, (3.4a) reduces to

$$\mathscr{L}^2\phi + \theta' = 0, \tag{6.2}$$

while (3.4b) remains the same. The corresponding algebraic eigenvalue problem, now of dimensions $N \times N$, then becomes

$$\left.\begin{aligned} \mathbf{A}\mathbf{x} &= \lambda \mathbf{x}, \\ \mathbf{A} &= [\mathbf{J} - \mathbf{K}\mathbf{F}^{-1}\mathbf{G}] + i\alpha Ra[\mathbf{V} - \mathbf{U}\mathbf{F}^{-1}\mathbf{G}], \\ \mathbf{x}^T &= (b_1, b_2, \ldots, b_N), \\ \lambda &= -i\alpha c Ra, \end{aligned}\right\} \tag{6.3}$$

where the component matrices of $\mathbf{A}$ are given in the appendix. The system (6.3) was solved to give the $Pr = \infty$ stationary curves shown in figures 7 and 9. As expected, the α_c^S and Ra_c^S curves for infinite Pr are almost indistinguishable from those for $Pr = 1000$.

It is interesting to note that neutrally stable travelling-wave solutions of (6.3) could not be obtained. However, examination of the eigenvalue spectrum, for $\gamma = 10$, revealed that the second mode represents a stable travelling wave of exactly the same type as that found by Gill & Davey (1969), for the buoyancy layer, in the limit $Pr \to \infty$ with $Pr\hat{R}$ fixed [see (3.6a–d)]. The absence of neutrally stable solutions, under the above limit, led Gill & Davey to examine the alternative case $Pr \to \infty$ with $Pr^{\frac{1}{2}}\hat{R}$ fixed, for which travelling-wave instability does exist. As mentioned above, Gill & Kirkham (1970) later studied a similar limit for the vertical slot and found travelling-wave instability but no stationary instability. Gill & Kirkham's limit was investigated in the present work also and, again, no neutrally stable stationary solutions were found.

The magnitudes of the critical parameters and power integral components for $Pr = 1000$ are given in table 3. The disturbance kinetic energy for travelling-wave instability and stationary instability is derived from the buoyancy source term, Σ_2, with the Reynolds stresses, represented by $Gr\Sigma_1$, providing a rather small, negative contribution to the kinetic energy in both cases. However, note that, in the domain in which stationary instability predominates, the relative contribution to the disturbance potential energy from the term $Gr\Sigma_5$, which involves the horizontal base flow temperature gradient, is larger for the stationary modes than for the travelling modes.

7. Discussion

In this paper, the instability of steady natural convection of a stably stratified fluid between vertical surfaces maintained at different temperatures has been investigated. The magnitude of the stable vertical stratification, represented by the parameter γ, and the value of the fluid Prandtl number, Pr, were found to have a strong influence upon the type and character of the instability. At both low and high Prandtl numbers, a change in the mode of instability occurs if the vertical stratification is increased beyond a certain level; that is, if γ exceeds a certain value denoted by γ_1. The magnitude of γ_1, as well as the nature of the transition in the mode of instability, depends upon the value of Pr. If $Pr \leqslant 12{\cdot}7$, then the critical disturbance modes are stationary if $\gamma < \gamma_1$, but they are travelling waves if $\gamma > \gamma_1$. In this range of Prandtl numbers, γ_1 decreases as Pr increases until $Pr = 12{\cdot}7$, at which point $\gamma_1 = 0$ and travelling waves determine the onset of instability for all γ in the interval $0 \leqslant \gamma \leqslant 15$. At high Prandtl numbers, the critical modes are travelling waves if $\gamma < \gamma_1$, but, if $\gamma > \gamma_1$, they are stationary. In the large Prandtl number case, the value of γ_1 decreases as Pr increases from 50 to 1000. However, in the limit $Pr \rightarrow \infty$ with Ra fixed, travelling-wave instability disappears altogether, and so, in this case, there is no transition value of γ.

When $Pr < 12{\cdot}7$ and $\gamma < \gamma_1$, the critical Grashof number, Gr_c^S, increases as γ increases, and there is a weak dependence of Gr_c^S upon Pr. The energy for stationary instability at low to moderate Pr is derived mainly from the base flow velocity field through the action of disturbance Reynolds stresses at the midplane between the upward and the downward flowing convective streams. Buoyancy forces work to enhance the instability when γ is small and to retard it when γ becomes sufficiently large. The stabilizing effect of an increase in the vertical stratification derives from a corresponding decrease in the velocity gradient at the centre-line of the channel (see figure 2).

The travelling-wave regime, for any given value of $Pr \leqslant 12{\cdot}7$, is divided into two subdomains. The first is defined as the interval $\gamma_1 \leqslant \gamma \leqslant \gamma_2$, where γ_2, which decreases with increasing Pr, is the value of γ at the minimum point of the appropriate critical curve for Gr_c^T (see figure 3). Within this interval, Gr_c^T decreases as γ increases, and both Gr_c^T and Ra_c^T are strongly dependent upon Pr. The second subdomain corresponds to the region $\gamma > \gamma_2$, in which Gr_c^T increases with increasing γ. One of the most interesting characteristics of the second subdomain is the rather small dependence of Ra_c^T upon Pr. For the Prandtl numbers $0{\cdot}73$–$12{\cdot}7$, the variation in Ra_c^T, at a particular value of γ, is less than 20% for $8 \leqslant \gamma \leqslant 15$. In both subdomains of the travelling-wave regime, the instability is almost entirely buoyancy driven, except for low values of Pr, in which case shear instabilities of the critical-layer type can occur if γ is not too large. It also should be noted that, at comparable values of Gr above the critical value, the growth rates of unstable travelling waves are significantly smaller than those for stationary disturbances.

	Experiment					
Investigators	Fluid	Pr	h	Gr_c	α_c	$\alpha_c c$
Elder (1965)	Silicone oil	1000	19	$3{\cdot}3 \times 10^2 \pm 30\,\%$	†	0
Vest & Arpaci (1969)	Air	0·71	33·33	$8{\cdot}7 \times 10^3$ } $\pm 10\,\%$	2·74	0
	Silicone oil	900	20	$4{\cdot}11 \times 10^2$ } $\pm 10\,\%$	3·5	0
Hart (1971)	Water	6·7	37·04	$1{\cdot}5 \times 10^4$ } $\pm 6\,\%$	†	†
	Water	6·7	25	$1{\cdot}94 \times 10^4$ } $\pm 6\,\%$	2·1	$6{\cdot}7 \times 10^{-3}$

Theory: $\tau h = \frac{1}{2}$, $\gamma = (Ra/8h)^{\frac{1}{4}}$

γ	Pr	h	Gr_c	α_c	$\alpha_c c$
6·91	1000	19	$3{\cdot}47 \times 10^2$	2·65	0
2·21	0·71	33·33	$8{\cdot}92 \times 10^3$	2·76	0
6·89	900	20	$4{\cdot}00 \times 10^2$	2·59	0
4·32	6·7	37·04	$1{\cdot}53 \times 10^4$	1·40	$5{\cdot}84 \times 10^{-3}$
4·73	6·7	25	$1{\cdot}20 \times 10^4$	2·00	$7{\cdot}33 \times 10^{-3}$

† Not determined.

TABLE 4. Comparison of theoretical results with available experimental data.

One of the most important findings of this study is the transition from travelling-wave to stationary instability which occurs at high Prandtl numbers. Stationary critical modes at high Prandtl numbers have been reported previously only by Vest & Arpaci (1969), but, as mentioned in §1, an error in their analysis has cast some doubt on their theoretical results. They omitted the term $-4\gamma^4\phi'$ in (3.4b), in which case the potential energy source term $Gr\Sigma_4$, in (4.1b), would be absent. As shown in table 3, $Gr\Sigma_4$ is strongly negative in the stationary regime and, therefore, not negligible.

The variation of Gr_c^S with γ at high Prandtl numbers is qualitatively similar to the variation of Gr_c^T with γ at low to moderate Prandtl numbers. Also, the critical Rayleigh number, Ra_c^S, in the large Prandtl number case has the same weak dependence upon Pr, in the subdomain $\gamma > \gamma_2$, as does Ra_c^T for the lower Prandtl numbers. However, in both the travelling-wave and the stationary regime, instability at large Pr is dominated by the effects of buoyancy.

Instabilities of the flow in the vertical slot were observed experimentally by Elder (1965), Vest & Arpaci (1969), and Hart (1971). A series of computations was performed for values of Pr and h (aspect ratio) appropriate for their experiments. The stratification parameter, γ, corresponding to a given aspect ratio and Rayleigh number was calculated using (2.4d) and the approximate relation $\tau h = \frac{1}{2}$ (see Elder 1965). The experimental and the predicted values for Gr_c, α_c, and c are listed for comparison in table 4. The theoretical results for stationary instability in the near-conduction regime ($Pr = 0{\cdot}71, \gamma = 2{\cdot}21$) are quite close to the experimental values determined by Vest & Arpaci (1969). In this case, the weak, stabilizing effect of the vertical stratification is reflected in the fact that Gr_c is about 10 % above its pure conduction value at $\gamma = 0$. The computed value for Gr_c for travelling-wave instability in water ($Pr = 6{\cdot}7$) compares well with the experimental value obtained by Hart (1971) for the larger of the two aspect ratios used in his experiments, but it is about 40 % lower than the experimental value for the smaller aspect ratio. However, even in the latter case, the theoretical and experimental values of the critical wavenumber, α_c, and critical frequency, $\alpha_c c$, are in reasonable agreement. Hart also found such agreement for the wavenumber and frequency for the case $h = 25$ but, in his analysis, he used the relation $\tau h = 0{\cdot}62$ and applied a small, empirically determined correction factor to the parameter γ. Thus, his theoretical results cannot be compared directly with those given in table 4. Nevertheless, it is worthwhile noting that his computed value of Gr_c for $h = 25$ is only about 10 % higher than ours, while for $h = 37\cdot04$ it is about 40 % lower. These differences are not surprising, because, as can be seen in figure 3, Gr_c varies significantly within the small range of γ covered by his experiments.

As mentioned in the introduction, experimental observations of stationary instabilities in high Prandtl number fluids have been in conflict with previous theoretical predictions of travelling-wave instability at large Pr (Gill & Kirkham 1970). Also, de Vahl Davis & Mallinson (1975) have found steady solutions of the full, nonlinear Boussinesq equations in a finite vertical slot, for $Pr = 1000$, at values of Gr_c slightly greater than the experimentally determined values. These solutions have the form of a multicellular secondary flow superimposed upon the (approximately) parallel base flow. De Vahl Davis & Mallinson suggested that the failure of the linear stability theory to predict the onset of stationary instability at large Pr might be due to the assumptions of a parallel base flow and an infinitesimal disturbance amplitude. However, as pointed out in the previous section, the large Pr limit studied by Gill & Kirkham simply does not admit neutral stationary solutions. As shown in table 4, the values for Gr_c^S obtained in the present study are in very good agreement with the experimental values reported by Elder (1965) and by Vest & Arpaci (1969). The value of 3·5 for the critical wavenumber given by Vest & Arpaci is somewhat higher than the theoretical value, but it should be pointed out that the neutral curve corresponding to their experimental parameters is rather flat near its minimum point. The neutral Grashof number at $\alpha = 3\cdot5$ was found to be $Gr_N = 4\cdot14 \times 10^2$, which is still quite close to the experimental result for Gr_c.

An estimate of the limiting value of the aspect ratio, h, required for a transition in the mode of instability can be obtained from (2.4d) and the approximate relation $\tau h = \frac{1}{2}$. For transition to travelling-wave instability in water ($Pr = 6\cdot7$, $\gamma_1 = 4\cdot0$), we find $h_1 \simeq 97$, whereas, for transition to stationary instability in oil ($Pr = 1000$, $\gamma_1 = 6\cdot6$), the result is $h_1 \simeq 44$. The magnitudes of h_1 computed for each case suggest that it might be possible to verify both types of transition experimentally.

A final comment regarding the recent theoretical paper by Mizushima & Gotoh (1976), which pertains to the subject of the present work, is in order. In this paper, stability calculations were performed for the case $Pr = 7\cdot5$, with γ ranging from 5·6 to 8. These parameter values are within the regime for travelling-wave instability. Denoting their stratification parameter by m, and their critical Grashof number and critical wavenumber by $\overline{Gr}_c$ and $\bar{\alpha}_c$, respectively, the appropriate transformations between their parameters and ours are as follows: $\gamma = 2m$, $\alpha = 2\bar{\alpha}$, $Gr_c = 16\overline{Gr}_c$. In table 5, the transformed critical values reported by Mizushima & Gotoh are contrasted with those found in the current study. The values of Gr_c obtained from the asymptotic relation for $Pr = 7\cdot5$ are also shown. Clearly, our results are quite different from those of Mizushima & Gotoh, our value of Gr_c at $\gamma = 5\cdot6$ being lower than theirs by more than a factor of 5. However, our value of Gr_c at $\gamma = 8$ is within 5 % of the asymptotic value. Mizushima & Gotoh derived the same asymptotic relation, in terms of their scaling, as that given in the table, but they did not provide a comparison of their tabulated critical values with those predicted by the asymptotic formula. Their curve for Gr_c is shown to merge smoothly with the large γ asymptote at the value $\gamma = 8$, but, unfortunately,

γ	Present study Gr_c	Present study α_c	Mizushima & Gotoh (1976) Gr_c	Mizushima & Gotoh (1976) α_c	Asymptotic relation $Gr_c = 42\gamma^3$
5·6	10673	2·72	56000	1·4	7376
6·0	11742	2·88	38400	2·2	9072
7·0	15957	3·22	41600	2·8	14406
8·0	22548	3·53	54400	3·2	21504

TABLE 5. Comparison of results of the present study with those of Mizushima & Gotoh (1976). $Pr = 7{\cdot}5$.

this cannot be reconciled with the figures given in table 5. Although the numerical solutions obtained in the current study are, of course, approximate ones based upon the particular trial functions used in the Galerkin method, the validity of the results is supported by numerous checks made on the convergence, accuracy, and consistency of the computations. Mizushima & Gotoh did not provide numerical examples of the convergence or accuracy of their computational method and, thus, it is not possible to identify the source of the discrepancies between their results and those reported here.

The author is indebted to Professor Chia-Shun Yih for his advice and encouragement during the course of this study. This work constitutes part of a Ph.D. thesis submitted to the Department of Applied Mechanics and Engineering Science in the University of Michigan. It was supported by the National Science Foundation and the office of Naval Research. Part of the computations were performed in the Computing Center of Argonne National Laboratory. Special thanks are due to Mrs Emma Taylor and to Mrs Debby Weck for typing the manuscript.

Appendix

The coefficient matrices of the linear algebraic system (5.4) are written in the form

$$\mathbf{A} = \begin{bmatrix} \mathbf{F} & \mathbf{G} \\ \mathbf{K} & \mathbf{J} \end{bmatrix} + i\alpha Gr \begin{bmatrix} \mathbf{E} & 0 \\ \mathbf{U} & \mathbf{V} \end{bmatrix}, \tag{A 1}$$

$$\mathbf{B} = \begin{bmatrix} \mathbf{C} & 0 \\ 0 & \mathbf{I} \end{bmatrix}, \tag{A 2}$$

where the elements of the various submatrices are defined by

$$\left.\begin{aligned} F_{mn} = \langle \phi_m, \mathscr{L}^2\phi_n\rangle, \quad G_{mn} = \langle \phi_m, \theta_n'\rangle, \quad K_{mn} = -\left(\frac{4\gamma^4}{Pr}\right)\langle \theta_m, \phi_n'\rangle, \\ J_{mn} = Pr^{-1}\langle \theta_m, \mathscr{L}\theta_n\rangle, \quad E_{mn} = -\langle \phi_m, (W\mathscr{L} - W'')\phi_n\rangle, \quad U_{mn} = \langle \theta_m, \Theta'\phi_n\rangle, \\ V_{mn} = -\langle \theta_m, W\theta_n\rangle, \quad C_{mn} = \langle \phi_m, \mathscr{L}\phi_n\rangle, \quad I_{mn} = \delta_{mn}. \end{aligned}\right\} \tag{A 3}$$

The power integral quantities E_k, E_p, and Σ_1 to Σ_6, which occur in (4.1 a, b), are given by

$$\left.\begin{aligned} E_k = -\tfrac{1}{2}\mathbf{a}^{*T}\mathbf{C}\mathbf{a}, \quad E_p = \tfrac{1}{2}\mathbf{b}^{*T}\mathbf{b}, \quad \Sigma_1 = -\tfrac{1}{4}(i\alpha)[\mathbf{a}^{*T}\mathbf{E}\mathbf{a} - \mathbf{a}^T\mathbf{E}\mathbf{a}^*], \\ \Sigma_2 = -\tfrac{1}{4}[\mathbf{a}^{*T}\mathbf{G}\mathbf{b} + \mathbf{a}^T\mathbf{G}\mathbf{b}^*], \quad \Sigma_3 = -\tfrac{1}{2}\mathbf{a}^{*T}\mathbf{F}\mathbf{a}, \quad \Sigma_4 = -(4\gamma^4/Ra)\Sigma_2, \\ \Sigma_5 = \tfrac{1}{4}(i\alpha)[\mathbf{b}^{*T}\mathbf{U}\mathbf{a} - \mathbf{b}^T\mathbf{U}\mathbf{a}^*], \quad \Sigma_6 = \tfrac{1}{2}\mathbf{b}^{*T}\mathbf{J}\mathbf{b}. \end{aligned}\right\} \tag{A 4}$$

REFERENCES

BATCHELOR, G. K. 1954 Heat transfer by free convection across a closed cavity between vertical boundaries at different temperatures. *Quart. Appl. Math.* **12**, 209–233.

BERGHOLZ, R. F. 1976 Ph.D. thesis, Dept. of Applied Mechanics and Engineering Science, University of Michigan.

BIRIKH, R. V. 1966 On small perturbations of a plane parallel flow with a cubic velocity profile. *Prikl. Mat. Mekh.* **30**, 356–361.

BIRIKH, R. V., GERSHUNI, G. Z., ZHUKHOVITSKII, E. M. & RUDAKOV, R. N. 1969 Stability of the steady convective motion of a fluid with a longitudinal temperature gradient. *Prikl. Mat. Mekh.* **33**, 958–968.

BIRIKH, R. V., GERSHUNI, G. Z., ZHUKHOVITSKII, E. M. & RUDAKOV, R. N. 1972 On oscillatory instability of plane-parallel convective motion in a vertical channel. *Prikl. Mat. Mekh.* **36**, 745–748.

ECKERT, E. R. G. & CARLSON, W. O. 1961 Natural convection in an air layer enclosed between two vertical plates with different temperatures. *Int. J. Heat Mass Transfer* **2**, 106–120.

ELDER, J. W. 1965 Laminar free convection in a vertical slot. *J. Fluid Mech.* **23**, 77–98.

ELDER, J. W. 1966 Numerical experiments with free convection in a vertical slot. *J. Fluid Mech.* **24**, 823.

GERSHUNI, G. Z. 1953 Stability of plane convective motion of a liquid. *Zh. Tekn. Fiz.* **23**, 1838–1844.

GILL, A. E. 1966 The boundary layer regime for convection in a rectangular cavity. *J. Fluid Mech.* **26**, 515–536.

GILL, A. E. & DAVEY, A. 1969 Instabilities of a buoyancy-driven system. *J. Fluid Mech.* **35**, 775–798.

GILL, A. E. & KIRKHAM, C. C. 1970 A note on the stability of convection in a vertical slot. *J. Fluid Mech.* **42**, 125–127.

GOTOH, K. & IKEDA, N. 1972 Asymptotic solution of the instability problem of channel flows with antisymmetric velocity profile. *J. Phys. Soc. Japan* **32**, 845–850.

GOTOH, K. & MIZUSHIMA, J. 1973 The stability of convection between two parallel vertical walls. *J. Phys. Soc. Japan* **34**, 1408–1413.

GOTOH, K. & SATOH, M. 1966 The stability of a natural convection between two parallel vertical planes. *J. Phys. Soc. Japan* **21**, 542–548.

HART, J. E. 1971 Stability of the flow in a differentially heated inclined box. *J. Fluid Mech.* **47**, 547–576.

KERCZEK, C. VON 1973 Ph.D. thesis, Johns Hopkins University.

KORPELA, S. A., GÖZÜM, D. & BAXI, C. B. 1973 On the stability of the conduction regime of natural convection in a vertical slot. *Int. J. Heat Mass Transfer* **16**, 1683–1690.

MACGREGOR, R. K. & EMERY, A. F. 1969 Free convection through vertical plane layers – moderate and high Prandtl number fluids. *J. Heat Transfer* **91**, 391–403.

MIZUSHIMA, J. & GOTOH, K. 1976 The stability of natural convection in a vertical fluid layer. *J. Fluid Mech.* **73**, 65–75.

MOLER, C. B. & STEWART, G. W. 1973 An algorithm for generalized eigenvalue problems. *SIAM J. Numer. Anal.* **10**, 241–256.

MORDCHELLES-REGNIER, G. & KAPLAN, C. 1963 Visualization of natural convection on a plane wall and in a vertical gap by differential interferometry. Transitional and turbulent regimes. *Heat Transfer Fluid Mech. Inst.*, pp. 94–111.

NACHTSHEIM, P. R. 1963 Stability of free-convection boundary-layer flows. *N.A.S.A. Tech. Note* D-2089.

OSHIMA, Y. 1971 Experimental studies of free convection in a rectangular cavity. *J. Phys. Soc. Japan* **30**, 872.

RUDAKOV, R. N. 1966 On small perturbations of convective motion between vertical parallel planes. *Prikl. Mat. Mekh.* **30**, 362–368.

RUDAKOV, R. N. 1967 Spectrum of perturbations and stability of convective motion between vertical planes. *Prikl. Mat. Mekh.* **31**, 376–383.

VAHL DAVIS, G. DE 1968 Laminar natural convection in an enclosed rectangular cavity. *Int. J. Heat Mass Transfer* **11**, 1675–1693.

VAHL DAVIS, G. DE & MALLINSON, G. D. 1975 A note on natural convection in a vertical slot. *J. Fluid Mech.* **72**, 87–93.

VEST, C. M. & ARPACI, V. S. 1969 Stability of natural convection in a vertical slot. *J. Fluid Mech.* **36**, 1–15.

WILKES, J. O. & CHURCHILL, S. W. 1966 The finite-difference computation of natural convection in a rectangular enclosure. *A.I.Ch.E. J.* **12**, 161–166.